2009 International Nuclear Atlantic Conference - INAC 2009
Rio de Janeiro,RJ, Brazil, September27 to October 2, 2009
ASSOCIAÇÃO BRASILEIRA DE ENERGIA NUCLEAR - ABEN
ISBN: **978-85-99141-03-8**

OPTIMIZATION OF DIGITAL CHEST RADIOGRAPHY USING COMPUTER MODELING AND VOXELS PHANTOMS

S.C.A. Correa[1,2], E.M. Souza[1,3], A.X. Silva[1], F.M. Milian[4], R.T. Lopes[1]

[1] Programa de Engenharia Nuclear – COPPE
Universidade Federal do Rio de Janeiro
Ilha do Fundão, Caixa Postal 68509
21945-970 Rio de Janeiro, RJ
scorrea@con.ufrj.br

[2] Centro Universitário Estadual da Zona Oeste, UEZO
Av. Manoel Caldeira de Alvarenga, 1203
23070-200 Rio de Janeiro, RJ

[3] Departamento de Geologia, Instituto de Geologia
Universidade Federal do Rio de Janeiro
Ilha do Fundão, 68509
21945-970 Rio de Janeiro, RJ

[4] Universidade Estadual de Santa Cruz, UESC
Salvador, Bahia

ABSTRACT

The purpose of this work is to use the Monte Carlo code MCNPX and the Female Adult voxel (FAX) and Male Adult voxel (MAX) phantoms to investigate how the dose and image quality in digital chest radiography vary with tube voltage (70-150 kV), anti-scatter methods (grid and air gap) and gender of the patient. The effective dose was calculated by ICRP60 and image quality was quantified by calculating the signal-difference-to-noise ratio for pathological details (calcifications) positioned at different locations in the anatomy. Calculated quantities were normalized to a fixed value of air kerma (5 μGy) at the automatic exposure control chambers. The results obtained in this work show that the air gap technique and lower tube voltages provide an increase in the digital image quality. Furthermore, this study has also shown that the detection of pathological details vary with the gender of the patient.

1. INTRODUCTION

Chest radiography is the most frequent radiographic examination performed in an x-ray department and, technically, it is one of the more difficult regions of the body to image with radiography because of the need to portray structures in tissues with both high and low attenuations.

With the introduction of digital imaging systems a range of potential improvements in image quality (IQ) has become possible. Important advantages associated with digital systems are the wide dynamic range and the image processing capabilities that allow image manipulation to improve visibility of anatomic details.

The most important factor affecting imaging performance for the range of tissue attenuations in different parts of a chest radiography is the spectral quality of the x-ray beam, determined primarily by the tube potential. Radiographic contrast relates to the choice of optimum

quality for the x-ray beam and is too important in determining whether the image signals, created by anatomic details, are perceptible against the background of the surrounding tissue. Since spectral sensitivities of digital detectors are different from those of conventional rare-earth screen-film systems, the spectral quality of the x-ray beam that will produce the best image with a digital detector is likely to be different for screen-film. Considering this, there is obviously a need for more optimization studies including both diagnostic quality of the digital images and the effective dose to the patient.

Previously we have developed a methodology for digital radiography simulation using the Monte Carlo code MCNPX [1-5]. This methodology takes into account the energy response by a BaFBr sensitive material image plate detector, the linear response curve of a 16 bit digital system and the presence of system noise such as electronic noise.

With this in mind, the purpose of this work is to use the above-mentioned methodology and the FAX and MAX voxel phantoms, to investigate how the dose and image quality in digital chest radiography vary with tube voltage (70-150 kV), anti-scatter methods (grid and air gap) and gender of the patient.

2. MODELED SYSTEM

The computer code used in this study was MCNPX version 2.5, the newest version of Monte Carlo MCNP [6]. Although several Monte Carlo codes can be used for these applications, MCNP has been chosen because it is largely employed and has already been validated in studies on radiation transport involving neutrons, photons, electrons, and more recently protons, in medical Physics and radiological protection. It is also a very versatile code, allowing users to specify parameters such as source type and geometric configuration, to indicate general conditions of the system such as size, shape, energy distribution and composition of the medium where radiation interaction takes place, and also to configure the information recording commands (tally).

The calculation of the absorbed dose to the organs and tissues of the human body has been performed by coupling the female and male voxel phantoms, FAX and MAX, respectively, by using MCNP. The recently introduced FAX and MAX phantoms [7,8] have organs and tissues adjusted to agree with the organ and tissue masses recommended by ICRP 89 [9] for the reference adult female and male, which specifies human characteristics that have a bearing on prospective calculations of doses originated in internal or external radioactive sources.

The coupling between the phantoms and MCNPX was carried out through a software called SCMS [10], a computational tool for the construction of geometries and anatomic models of medical images such as computed tomography (CT) and other similar digital images. SCMS interprets images and save this interpretation in an input file used by Monte Carlo code MCNPX in the simulation of radiation transport [11].

The energy spectrum of X-rays used as input parameter in the simulation of the radiation beams was obtained with the software SRS 78 [12], using a total filtration of 5mm aluminum, a tungsten anode with an angulation of 16° and tube voltages ranging from 70-150 kV. The energy spectrum was described in MCNPX code using 0.5 energy bins. The photons were emitted by a 0.1-cm-diameter plane circular source collimated into a cone of directions by

using the variance reduction technique called *source biasing* [6]. Lead collimators were modeled so as to define a square irradiation field at the image detector. The radiation field area was 36 x 36 cm^2, covering all the organs within the region of interest.

The photons emitted by the radiation source propagated through the air-filled medium before interacting with the phantoms. The effective doses were calculated through MNCPX's *F8 command and using the ICRP60 [13]. The dose values were normalized to an air kerma at the image detector of 5 μGy [14].

Two different techniques for reduction of the scattered radiation have been considered, namely the antidiffusion grid and the air gap. In order to study the first one, focused linear grid was modeled. The parameters of the grids included in this study are recommended by European Commission [15]. The table 1 present the parameters used to model the grid.

Table1. Grid Parameters.

Strip density (lines/cm)	Thickness of aluminum cover (μm)	Thickness of lead strips (μm)	Thickness of aluminum interspace (μm)	Grid ratio	Identification
40	**400**	**50**	**200**	**10**	**40/10/50**

The grid was placed after the phantom. The distance from the phantom to the posterior surface of a grid was kept at 1,5 cm. The distance between the grid and the focal point was set to 149 cm, while the distance from the image detector to the focal point was 150 cm. In the air gap technique, the distance from the focal point to the image detector was set to 300 cm and the air gap was equal to 30 cm.

In this study, every calculation was based on the generation of a number of histories large enough to guarantee a relative statistical error smaller than 0.05.

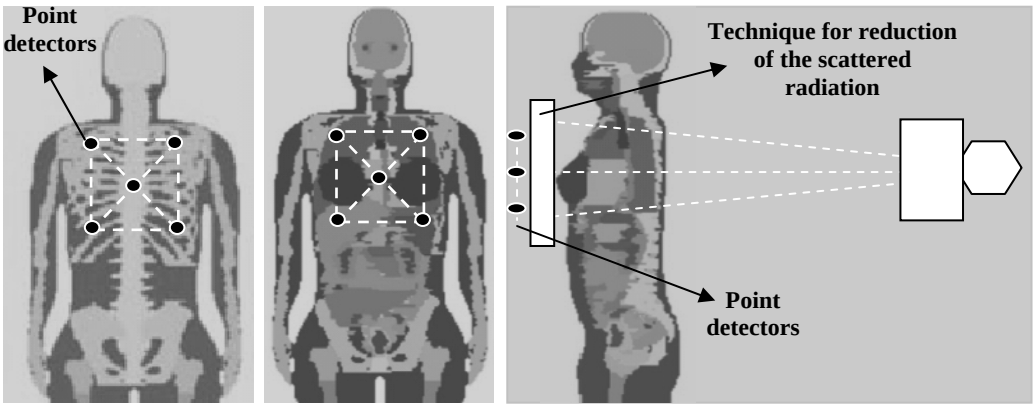

Figure 1. Locations of five point detectors.

The validation of the grid was accomplished through the calculation of the Primary Transmission (T_p), the Total Transmission (T_t), the Bucky Factor (BF) and the Contrast Improvement Factor (CIF), using the methodology and experimental values published by Chan et al. [16]. Validation was accomplished using a beam of photons generated by

applying a voltage of 80 kV to the X-ray tube, with a 2.5 mm thick Al filter and a pair of KODAK Lanex regular screens (Gd_2O_2S:Tb, 70 mg/cm^2 per screen). Table 2 compares the performance of the modeled grid used in this work with the grids studied experimentally by Chan et al. [16].

Table 2. Comparison of measured and simulated grid performance parameters.

Identification	Simulated grid				Experimental measuremensts [(a)]			
	T_t	T_p	BF	CIF	T_t	T_p	BF	CIF
40/10/50	0,172	0,623	5,81	3,60	0,170	0,620	5,88	3,65

(a) Chan et al.[16].

2.1 Modeling the Image Plate Detector

The MCNPX code [6] uses a set of point detectors close enough to each one to create an image based on the fluence of particles passing through each detector. Once the image function is activated, MCNPX creates a virtual two-dimensional pixel matrix perpendicular to the particle beam's central axis, at a selected distance from the (under) test subject, where millions of point detectors may be created, one detector for each pixel. These pixels work like cells in which the particles will be counted or their energies recorded. Each individual pixel in this matrix represents one pixel in the simulated image.

In order to consider the energy response by a BaFBr sensitive material image plate detector, the number of photons incident on the detector and the presence of system noise, the methodology for simulating computed radiographic images developed by our group [1-5] was considered.

2.2 Image Quality

The signal-difference-to-noise ratio (SdNR) for the single-exposure method [17] was used as the measure of physical image quality. This quantity is defined as:

$$SdNR = \frac{|I_B - I_L|}{\sigma_B} \tag{1}$$

where I_L and I_B refer to the intensity of the detector signal corresponding to a lesion and its background surrounding, respectively, and σ_B is the standard deviation of quantum noise in the background area.
The figure of merit (FOM) was calculated as the square of SdNR divided by the effective dose, E,

$$FOM = \frac{SdNR^2}{E} \tag{2}$$

Image quality was computed for a set of pathological details with 6 mm diameter included in the voxel phantoms at a specified location according to Figure 2. Table 3 gives the detail thickness and composition used in the calculations.

Table 3: Pathological details positioned at different locations in the anatomy.

Identification	Region	Thickness	Composition	Density (g/cm^3)
D1	Central pulmonary region	1 mm	CaO	3.3
D2	Central pulmonary region	2 mm		
D3	Retrocardial region	1 mm		
D4	Retrocardial region	2 mm		
D5	Apical pulmonary region	1 mm		
D6	Apical pulmonary region	2 mm		

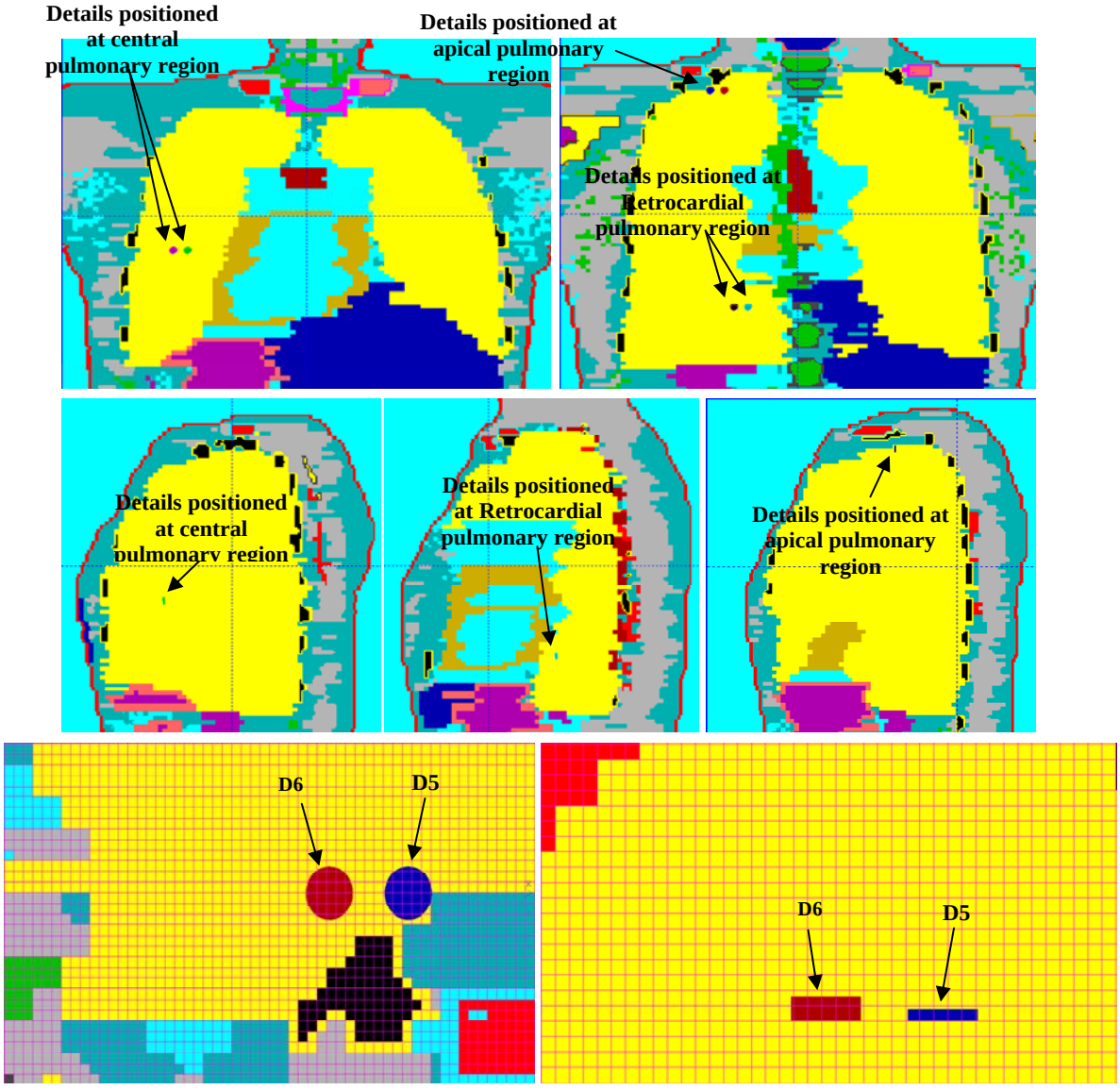

Figure 2. Localizations of the details included in the MAX phantom. Image obtained with the software Moritz.

3. RESULTS

Figures 3 and 4 show SdNR and FOM as a function of voltage. Independently of the techniques for reduction of the scattered radiation, both quantities are higher for details with 2 mm thickness. This behavior is due to an increase in the difference between the detector signal corresponding to a detail and its background surrounding with increase of thickness.

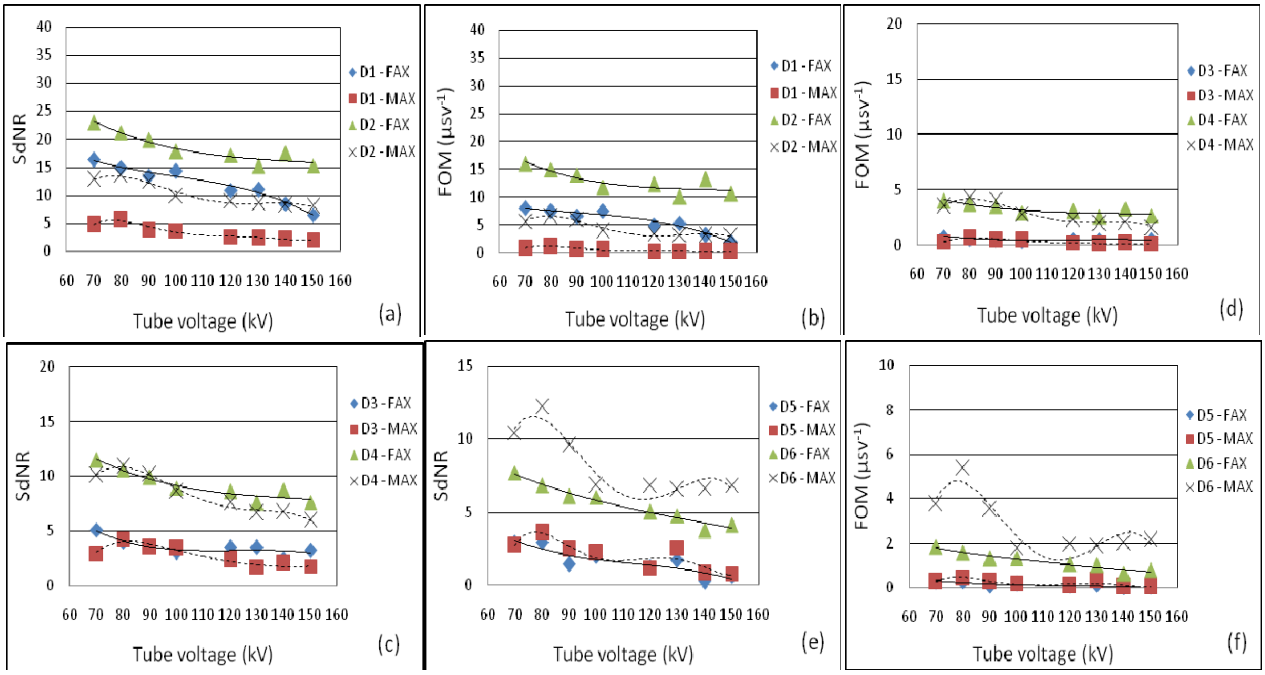

Figura 3: SdNR and FOM as a function of voltage to the FAX and MAX phantoms using grid technique. In (a) SdNR for central pulmonary region, (b) FOM for central pulmonary region, (c) SdNR for retrocardial region, (d) FOM for Retrocardial region, (e) SdNR for apical pulmonary region and (f) FOM for apical pulmonary region.

With the air gap technique, for the details located in the central pulmonary and retrocardial regions SdNR and FOM are higher in women. For the details located in the apical pulmonary region they are higher in men. This behavior is not similar to the grid technique. In this case, SdNR and FOM for details with 1 and 2 mm thickness located in the retrocardial pulmonary region and details with 1 mm thickness located in the apical pulmonary region do not vary with gender of the phantom.

In Figure 5 can be observed that both quantities (SdNR and FOM) are higher for the air gap technique, suggesting that the air gap is the superior scatter rejection technique. The transmission of primary radiation through the grid reduces the image quality and increases the bucky factor; this is avoided using the air gap technique. Figure 4 also shows that SdNR and FOM decrease with increasing tube voltage, indicating that lower tube voltages should be used for improve the quality image. For FAX, the FOM was higher at 70 kV and for MAX, it was higher at 80 kV.

The variations observed in the detection of subtle details in chest radiographs and in the best tube voltage value with the gender of the phantom, occur due male and female anatomy

present differences concerning the size and distribution of organs (Figure 6). It cause variations in anatomical background and consequently affect the detection of details.

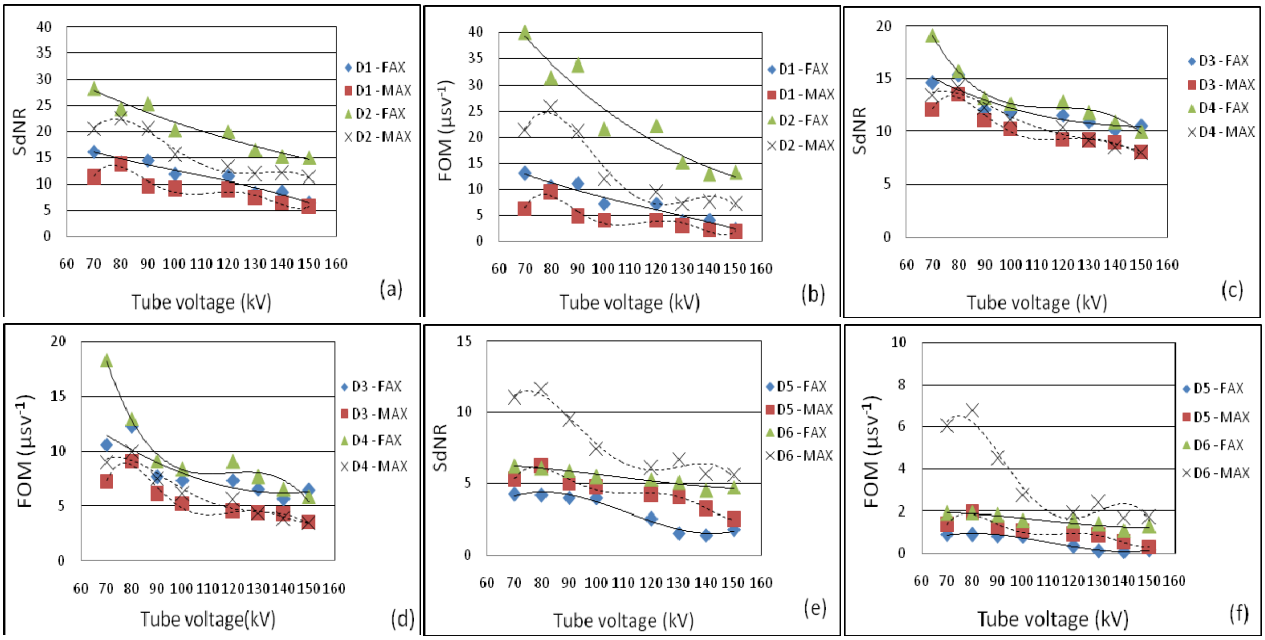

Figura 4: SdNR and FOM as a function of voltage to the FAX and MAX phantoms using air gap technique. In (a) SdNR for central pulmonary region, (b) FOM for central pulmonary region, (c) SdNR for retrocardial region, (d) FOM for Retrocardial region, (e) SdNR for apical pulmonary region and (f) FOM for apical pulmonary region.

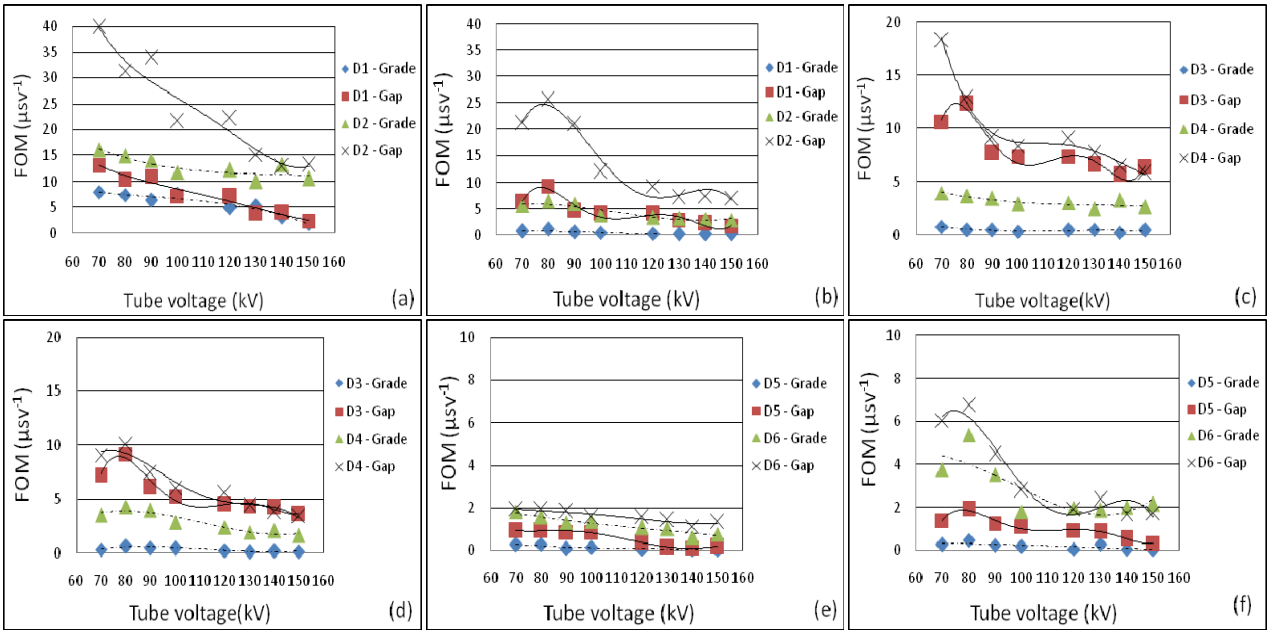

Figure 5: FOM as a function of voltage to the FAX and MAX phantoms using air gap technique and grid. In (a) FOM in central pulmonary region for FAX, (b) FOM in central pulmonary region for MAX, (c) FOM in retrocardial region with FAX, (d) FOM in retrocardial region with MAX, (e) FOM in apical pulmonary region with FAX and (f) FOM in apical pulmonary region with MAX.

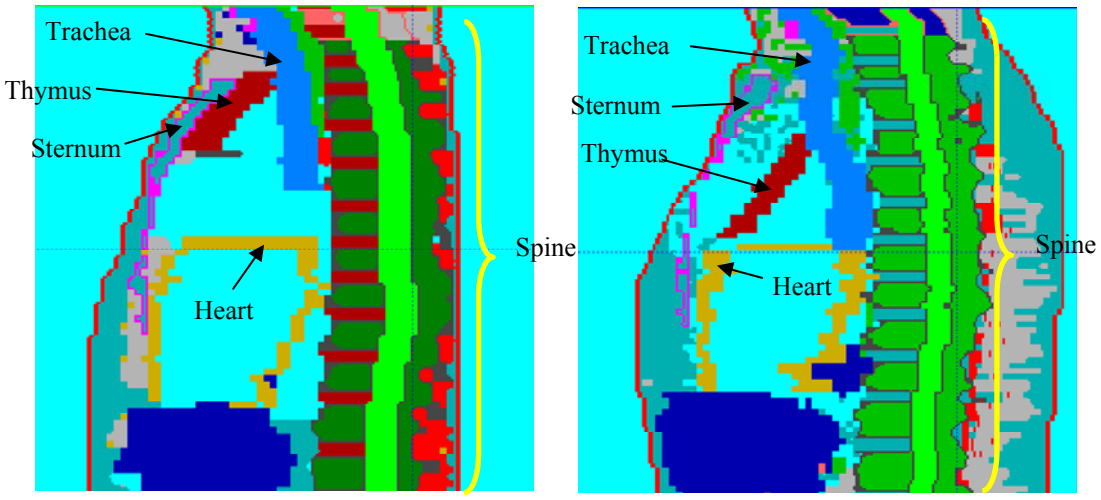

(a) (b)

Figure 6: differences concerning the size and distribution of organs with the gender of the phantom. In (a) FAX and (b) MAX. Image obtained with the software Moritz.

4. CONCLUSIONS

In all regions the air gap technique provides higher SdNR and FOM compared with the grid technique. Results also indicate that lower tube voltages should be selected since higher values of SdNR and FOM are obtained for details at the lower tube voltages. Finally, the results have also confirmed that the detection of pathological details vary with the gender of the patient.

ACKNOWLEDGMENTS

The authors wish to thank the financial support of the Conselho Nacional de Desenvolvimento Científico e Tecnológico (CNPq) and Fundação Carlos Chagas Filho de Amparo à Pesquisa do Estado do Rio de Janeiro (FAPERJ), Brazil.

REFERENCES

1. E.M. Souza, S.C.A. Correa, A.X. Silva, D.F. Oliveira, R.T. Lopes, "Methodology for Digital Radiography Simulation using the Monte Carlo Code MCNPX for Industrial Applications", *Applied Radiation and Isotopes*, **66**, pp. 587-592 (2008).
2. S.C.A. Correa, E.M. Souza, A.X. Silva, R.T. Lopes, H. Yoriyaz, "Dose-Image Quality Study in Digital Chest Radiography using Monte Carlo Simulation", *Applied Radiation and Isotopes*, **66**, pp. 1213-1217 (2008).
3. S.C.A. Correa, E.M. Souza, D.F. Oliveira, A.X. Silva, R.T. Lopes, C. Marinho, C.S. Camerini, "Assessment of Weld Thickness loss in Offshore Pipelines using Computed Radiography and Computational Modeling". *Applied Radiation and Isotope, DOI: 10.1016/j.apradiso.2009.05.015* (2009).
4. E.M. Souza, "Modelagem de Sistema e Procedimento para Radiografia Computadorizada OFFSHORE". *Tese de D.Sc.*, COPPE/UFRJ, Rio de Janeiro, RJ, Brasil (2008).

5. S.C.A. Correa, "Otimização da Dose e da Imagem Radiográfica Digital de Tórax usando Modelagem Computacional". *Tese de D.Sc.*, COPPE/UFRJ, Rio de Janeiro, RJ, Brasil (2009).
6. D.B. Pelowitz, Ed. MCNPX^{TM} User's Manual. Version 2.5.0., Los Alamos National Laboratory *Report LA-CP-05-0369* (2005).
7. R. Kramer, J.W. Vieira, H.J. Khoury, F.R.A. Lima, D. Fuelle, "All about MAX: a Male Adult Xoxel Phantom for Monte Carlo Calculation in Radiation Protection Dosimetry", *Phys. Med. Biol.*, **48**, pp. 1239-1262 (2003).
8. R. Kramer, H.J. Khoury, J.W. Vieira, E.C.M. Loureiro, V.J.M. Lima, F.R.A. Lima, G. Hoff, "All about FAX: a Female Adult Xoxel Phantom for Monte Carlo Calculation in Radiation Protection Dosimetry". *Phys. Med. Biol.*, **49**, pp. 5203-5216 (2004).
9. International Commition on Radiological Protection. *Basic Anatomical and Physiological Data for Use in Radiological Protection: Reference Values*. ICRP Publication 89 - Oxford: Pergamon Press (2003).
10. H. Yoriyaz, A. Santos, M. Stabin, "Absorbed Fractions in a Voxel-Based Phantom Calculated with the MCNP-4B Code", *Med. Phys.*, **27**, n. 7, pp. 1555-1562 (2000).
11. H. Yoriyaz, M. Stabin, A. Santos, "Monte Carlo MCNP-4B Based Absorbed Dose Distribution Estimates for Patient: Specific Dosimetry", *J. Nuc. Med.,* **42**, n. 4, pp. 662-669 (2001).
12. K. Cranley, B.J. Gilmore, G.W.A. Fogarty, L. Desponds, *Catalogue of Diagnostic X-Ray Spectra and Other Data. Institute of Physics and Engineering in Medicine.* Report 48, (1997).
13. International Commission on Radiological Protection. *Recommendations of the International Commission on Radiological Protection.* ICRP Publication 60, Oxford: Pergamon Press (1991).
14. S.C.A. Correa, E.M. Souza, A.X. Silva, H. Yoriyaz, R. T. LOPES, "AP and PA Thorax Radiographs: Dose Evaluation using the FAX Phantom", *International Journal of Low Radiation*, **5**, n. 3, pp. 237-255 (2008).
15. European Commission. *European Guidelines on Criteria for Diagnostic Radiographic Images.* Report EUR 16260 - CEC, Brussels (1996).
16. H. Chan, K. Doi, "Physical Characteristics of Scattered Radiation in Diagnostic Radiology: Monte Carlo Simulation Studies", *Med. Phys.*, **12**, pp. 152-165 (1985).
17. E. Samei, J.T. Dobbins, J.Y. Lo, M.P. Tornai, "A Framework for Optimising the Radiographic Technique in Digital X-Ray Imaging", *Radiation Protection Dosimetry,* **114**, n. 1-3, pp. 220-229, 2005.